

UDC 681.723.067.28:532.42/.44:681.785.42

MULTI-MODE MICROSCOPY USING DIFFRACTIVE OPTICAL ELEMENTS

Yan FENG – Louisa SCHOLZ – David LEE – Heather DALGARNO – David FOO – Lei YANG – Weiping LU – Alan GREENAWAY

Abstract: This paper discusses a range of phase-diversity and tracking applications that have been demonstrated experimentally, and will present an analysis of experimental errors associated with the system used. Simultaneous imaging in multiple imaging modes is demonstrated and the use of wavefront-sensing techniques to achieve nanometric depth resolution is reviewed.

Keywords: – diffractive optical elements
– 3D imaging
– phase diversity
– phase contrast

1. INTRODUCTION

Diffractive optical elements (DOEs) in the form of gratings can be used in simple attachments for commercial microscopes to record wide-field images focused simultaneously on multiple specimen depths. This allows simultaneous measurements in different phase-contrast modes (e.g. simultaneous bright-field and phase-contrast measurement) and other forms of simultaneous phase-diversity in microscope images. Simultaneity in measurement is important in applications for studies of rapidly changing objects in cell-biology, fluid-flow problems and other high-speed, 3D tracking applications.

Used to image unresolved particles in microscopy, the multi-focus image approach has been combined with wavefront-sensing techniques to demonstrate $\pm 8\text{nm}$ depth resolution from single data frames with high-flux objects. Modeling suggests that a depth-resolution accuracy of 30nm is achievable on sources such as single proteins, provided that 200 photons per data frame are available.

2. SIMULTANEOUS MULTI-MODE IMAGING IN MICROSCOPY

Combining a DOE with a conventional positive lens achieves multi-mode imaging by exploiting the well-known detour phase principle, i.e. that

radiation scattered from a distorted diffraction grating suffers a phase change dependent on the local distortion of the grating and the diffraction order considered [1]. Each of the diffraction orders forms an image by virtue of the conventional lens. Some of the possible image modes achievable are discussed below.

2.1. Controlling the intensity in multiple images generated with a DOE

The use of a phase-relief DOE to achieve multiple imaging modes simultaneously is greatly beneficial in terms of photometric efficiency, but the fraction of the energy from the illumination beam that is scattered into each of the DOE diffraction orders is dependent on the phase depth of the DOE. A binary-phase DOE with mark-space ratio of unity, made using a transparent material such as fused silica, scatters energy into the zero and ± 1 diffraction orders according to:

$$\begin{aligned} I_0 &= \cos^2\left(\frac{\pi\varepsilon(n-1)}{\lambda}\right); \\ I_{\pm 1} &= \frac{4}{\pi^2} \sin^2\left(\frac{\pi\varepsilon(n-1)}{\lambda}\right); \\ I_{\pm 1} &= \left(1 - \frac{8}{\pi^2}\right) \sin^2\left(\frac{\pi\varepsilon(n-1)}{\lambda}\right), \end{aligned} \quad (1)$$

where λ is the wavelength, ε the etch depth, n the material refractive index, the subscripts 0 and ± 1 indicate the energy scattered into the 0 and ± 1

diffraction orders and subscript l indicated the fraction of the input energy lost into higher diffraction orders. Most of the measurements described here use an etch depth selected to equalize the flux in the 0 and ± 1 diffraction orders, which requires an etch depth such that the phase in the trig functions of Eq. 1 correspond to $\varphi = 2.008$ rad. With this phase the 3 diffraction orders used each contain 28.84% of the flux and 13.45% of the flux is lost into higher diffraction orders. Figure 1 shows the energy in the diffraction orders as a function of φ .

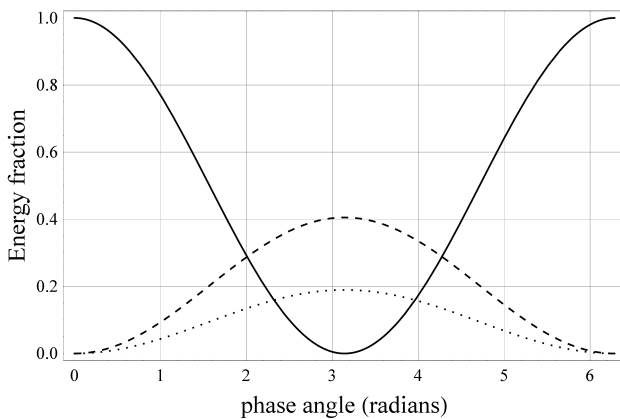


Figure 1. Plot showing the energy balance in the 0 (solid line), ± 1 diffraction orders (dashed) and the fraction of the flux lost into higher diffraction orders (dots), for a binary DOE structure of the sort used in our experiments.

Our DOEs are etched to balance the intensity in 3 images, where the solid and dashed lines intersect. Higher efficiencies can be achieved by using multi-level etches or continuous profiles, but these are 5-10 times more expensive than the binary gratings used here. The simple binary gratings that we describe put 84% of the light into useful images.

2.2. Multi-focus images

The use of quadratically-distorted DOEs to achieve simultaneous in-focus images of many specimen planes has been reported before [2-4]. In summary, a DOE in the form of an off-axis zone-plate imposes a different curvature on the incident wavefront in each diffraction order. Combined with a conventional positive lens, this provides multiple in-focus images on a single detector in which each DOE diffraction order focuses on a different specimen depth. The system thus provides a ‘z-

stack’ with no need for mechanical scanning and with the advantage that images at all depths are recorded during a single integration time. Such images have been recorded in bright-field, dark-field, phase-contrast, DIC and fluorescent imaging modes. A schematic of a DOE for multi-focus imaging in these imaging modes is shown in Figure 2(a). Combined with simple wavefront-sensing approaches, such data can provide real-time, 3D particle-tracking with nanometric accuracy [5, 6]. By crossing 2 DOEs at right angles, 9 images focused at different Z-depths can be achieved in a 3×3 matrix.

2.3. Phase-contrast images

Transparent objects change the phase of the transmitted light. This phase-shifted light is scattered out of the illumination beam but, excepting light scattered outside the aperture or the presence of optical aberrations, an image-forming lens recombines all scattered radiation at a point in the image conjugate to the specimen point from which it was scattered. The resulting image shows negligible contrast, but it is well known [e.g., 7] that changing the phase of the scattered beam relative to the un-scattered beam can deliver useful contrast levels and, for weak phase objects, this contrast can be reversed by changing the direction of the mutual phase shift between scattered and un-scattered wave (positive and negative phase contrast). By dislocation of a DOE structure in the region of the unscattered beam by one quarter period, the ± 1 diffraction orders give simultaneous positive and negative phase contrast. The contrast level can be adjusted by attenuating the un-scattered beam. When the object is not a weak phase object the contrast is not completely reversed if the mutual phase shift is reversed. This asymmetry in image contrast can be exploited to assist in the reconstruction of the phase of objects for which the weak-scattering approximation fails. DOEs suitable for producing phase-contrast images are shown in Figure 2(b) and 2(c). By adjusting the etch depth, the zero-order image can be made dark-field (etch depth producing π radians) or bright field – where the etch depth can be used to attenuate the strength of the unscattered beam in the positive and negative phase contrast images (in ± 1 diffraction orders). Using curved and dislocated DOE structures, the 3-D imaging can be combined with phase-contrast imaging (Figure 2(d)).

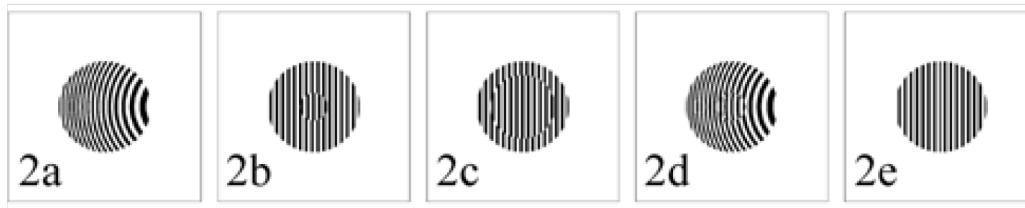


Figure 2. Schematic DOEs for multi-mode imaging measurements: 2a, multi-focus (simultaneous z-stack); 2b, simultaneous negative phase contrast, bright-field, positive phase contrast (axial illumination); 2c, simultaneous negative phase contrast, bright-field, positive phase contrast (conical illumination); 2d, combined phase contrast and multi-focus imaging; 2e, Hilbert-transformation.

2.4. Other imaging modes

By dislocating the gratings along a central line (in either direction) the Hilbert transform of the complex amplitude produced by the object can be measured. A suitable DOE structure is shown in Figure 2(e). However, it should be noted that the images produced have been of curiosity value rather than useful – but they do indicate the flexibility achievable.

2.5. Imaging modes - summary

The use of a 1:1 image relay combined with a DOE provides a low-cost and flexible approach to the implementation of image capture involving several different imaging modes. These modes include imaging multiple object depths simultaneously on a single camera, combinations of positive, negative phase contrast with bright-field/dark-field imaging or novel mathematical transforms, such as the Hilbert transform. Other phase filters, such as cubic-mask extended depth of focus, or double-helix imaging [8], may be implemented in this arrangement.

3. ERRORS IN IMPLEMENTATION OF DOE-BASED, MULTI-MODE IMAGING

Errors affecting the accuracy of DOE-based multi-mode imaging can be treated under two convenient headings – those arising from defects in the DOE structures and those arising from conventional optics. Experimentally, all of the DOE-based schemes discussed here are used with an imaging system based on an optical relay between the usual microscope detector port and the multi-mode image plane (to which the users' chosen camera is displaced).

Figure 3 is a schematic of the optical relay. Positioning the DOE one focal length behind the lens ensures that all images have identical magnification – avoiding the need for re-scaling. Typically we use a re-imaging lens of $f \sim 75\text{mm}$ focal length, so the total optical length of this system is $\sim 300\text{mm}$. Varying the grating period changes the separation of the images – allowing full exploitation of any camera format.

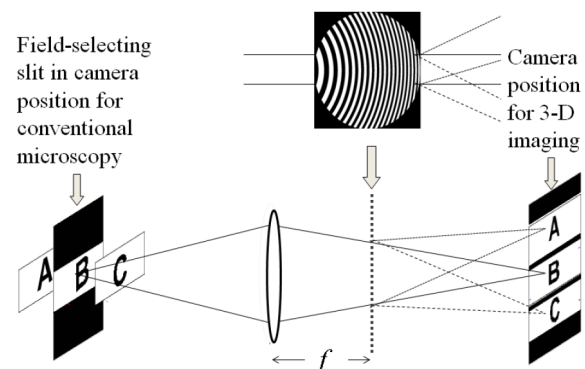


Figure 3. Schematic for multi-focal imaging, showing the quadratic curvature of the binary-phase DOE and a slit used to ensure that the separate z-plane images do not overlap.

3.1. Mis-placing the DOE

For 3D imaging, placing the DOE one focal length behind the lens (Figure 3) ensures that the images in all diffraction orders have equal magnification. The optics were modeled (Figure 4) with Zemax ray-tracing software and include a bandpass filter limiting the wavelength range to $530 \pm 5\text{nm}$, two 150mm achromatic lenses acting as a 1:1 relay, and the quadratically curved DOE. The DOE has a 1mm thick fused silica substrate, period $20\mu\text{m}$, and a focal

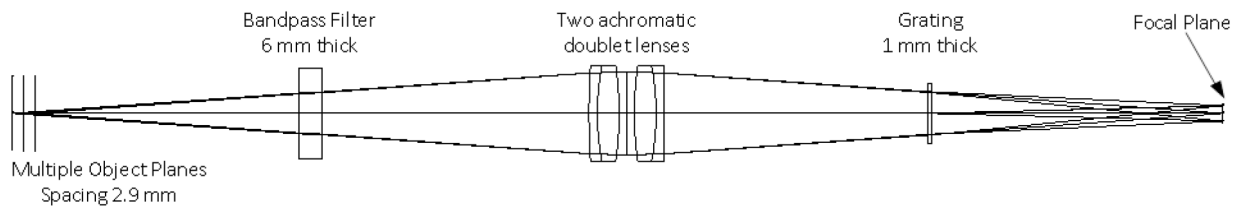


Figure 4. Optical ray-trace diagram of the 3D imaging system.

length of $\pm 2\text{m}$ for diffraction orders ± 1 . The model includes an $\text{NA}=0.6$, $\times 40$ microscope objective and tube lens not shown in Figure 4. The object plane separation caused by the DOE is $\pm 2.9\text{mm}$ at the entrance to the relay optics equivalent to $-1.86\mu\text{m}$ and $+1.80\mu\text{m}$ at the specimen. For a $40\times$ microscope objective, the beam entering the relay optics has a focal ratio of $F/26$. The predicted P-V wavefront error in the relay optics is less than 0.01 waves on-axis (zeroth order), and ~ 0.12 waves at the edges of the detector (± 1 orders). The system is thus diffraction limited, with an Airy disk at focus $\sim 34\mu\text{m}$ diameter (~ 5 Nyquist-spaced detector pixels). Magnification differences $\sim 0.25\%$ between the images in the 3 diffraction orders are achievable experimentally using test objects on the microscope.

3.2. Assessing focus

The Strehl ratio and the image sharpness [6, 9] are both maximum for a diffraction-limited image. The Strehl is hard to measure experimentally but, as shown in Figure 5, the Strehl and image sharpness maxima coincide accurately. In our experiments [5, 6] we use the maximum image sharpness (equally

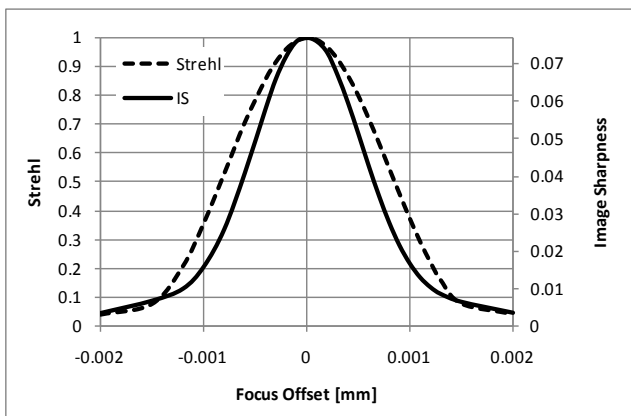


Figure 5. Plot showing the through focus variation in Strehl ratio (dashed line) and image sharpness (IS - solid line) versus defocus at the microscope image plane.

applicable to extended incoherent sources) as an indicator of ‘best focus’.

These curves are produced from the Zemax software and model a displaced point source. The peak Strehl and image sharpness values occur at the optimum focus where the wavefront error is minimized. The image sharpness falls to 50% of its peak value when the P-V wavefront aberration reaches 0.34 waves – in this example at $0.65\mu\text{m}$ focus offset.

3.3. Spacing of the z-stack

The spacing of the axial foci is measured using the image sharpness and related back to a microscope specimen using the square of the magnification. Ray-tracing for catalogue lenses gives image-plane z-separation exceeding thin-lens calculations [2-4] by $\sim 3.6\%$.

3.4. Image z-plane intensity variation

The DOE moves the principal plane of the objective lens in the diffraction orders [4], slightly changing the numerical aperture (NA) for each plane in the 3D imaging mode (objects closer to the objective are imaged with a slightly-higher NA). This effect was noted experimentally [5], and the observed changes are consistent with ray-tracing analysis. The induced flux variation in the multi-focal images can be $\sim 4\%$ percent, but is easily assessed from measurements.

3.5. Aberrations induced by optics

Deviations in the thickness of the cover slip from that for which the microscope objective was designed is the principal source of spherical aberration, but small amounts of additional spherical aberration and defocus are due to the interference filter and the substrate into which the DOE has been etched. In addition, the use of diffraction by the DOE to separate the images recorded in different image modes means that the images in the ± 1

diffraction orders strike the camera at slight angles, and this breaking of the axial symmetry induces small amounts of coma aberration [2]. Ray-tracing analysis indicates that these effects reduce the Strehl in the ± 1 diffraction- order images by less than 1% for monochromatic imaging.

3.6. Dispersion

The DOEs used in multi-mode imaging are dispersive, so chromatic effects degrade performance in the ± 1 order images. Over a 10nm bandwidth the peak position for the ± 1 order images can move by one half of the width of a diffraction-limited spot (2-3 pixels for the system in Figure 4). This chromatic blur depends on the DOE grating period, the focal length of the re-imaging lenses and the spectral profile used. In phase-contrast imaging, DIC and dark-field imaging modes, one can use a sufficiently-narrow band illumination that chromatic effects are negligible. For fluorescent imaging the fluorophore bandpass may reach 30-50nm, and the use of the full fluorescence spectrum is important to minimize photo-damage, therefore chromatic correction is required. For the instantaneous z-stack images the changing period of the DOE structure may be used to correct the chromatic effects due to the wavelength-dependent angle of the diffraction orders. Pre-dispersion of the light before it is incident on the DOE can correct this dispersion, even for unfiltered white light illumination [3], and work is continuing to effect this chromatic correction in telecentric imaging and with high efficiency.

3.7. DOE etch-depth error

The energy balance between different diffraction orders is, as shown in Figure 1, dependent on the phase-profile of the DOE. To achieve the desired intensity balance between the images in each diffraction order it is important to control the etch depth. We design the DOEs but these are etched into a fused silica substrate commercially. The etch depth is reasonably uniform across each set of 16 DOEs that are etched together, but it is important to know how precisely a target etch depth can be achieved in order to determine the energy imbalance between the images. On a relatively small sample of etch runs the depth error appears to be typically ~ 2 nm with just one example exceeding 7nm error. To model the effect of such errors, we assume that the etch-depth, ε , is Normally distributed with the

target mean and a given standard deviation. Eq (1) then allows us to estimate the energy balance. The resulting integrals are not easily solved analytically, but the numerical integration is straightforward. This indicates that the energy balance between the zero and ± 1 diffraction orders is $< 4\%$, with a 95% probability, if the standard deviation on the etch depth error is < 2 nm. Thus, we can use a single etch with a high certainty of getting the correct energy balance for the selected wavelength.

3.8. Surface roughness

The effect of residual roughness in the DOE etch can be analysed using the Marechal approximation [see, e.g. 7] to assess its effect on the Strehl ratio. The residual roughness can be measured by stylus contact and, in the examples fabricated thus far, has an rms amplitude of ~ 3 nm. The effect on the optical wavefront also depends on the scale length of the error, since roughness with a scale length significantly below one wavelength will tend to be averaged, but we assume that the rms roughness applies equally at all lateral scales. A plot of the Strehl for small errors is shown in Figure 6.

The Marechal approximation gives the Strehl ratio as the negative exponential of the phase variance $S = \exp(-\sigma_\varphi^2)$, which is easily calculated. As Figure 6 shows, the Strehl remains > 0.99 provided that $\sigma_\varepsilon < 20$ nm, so the roughness does not present a problem in terms of system performance.

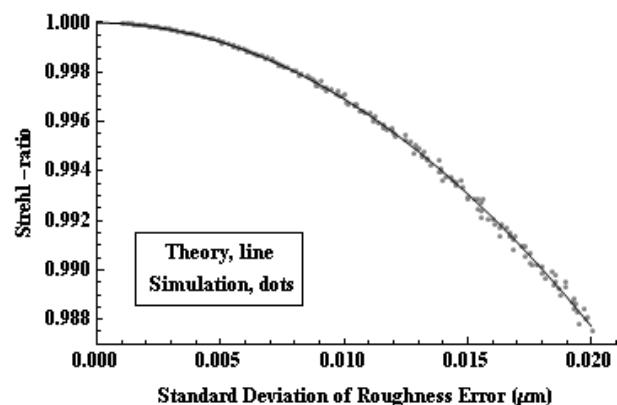


Figure 6. The Strehl ratio as a function of the roughness error standard deviation.

3.9. DOE plotting error

Our DOEs are designed using GDSII and the etch masks are made using a laser plotter, followed by a

dry-etch of the fused silica. The binary masks are plotted with a $1\mu\text{m}$ resolution and typical grating periods are $25\mu\text{m}$. Particularly in the case of the zone plates used to produce multi-focus images, the curved features in the zone-plate are plotted in straight-line segments, which is a source of error. To analyse the effects of this, we model the grating as the sum of an idealized phase grating plus an array of 'top hat' functions located at the transitions between the etched and un-etched regions and of positive- or negative-going nature dependent on whether the error represents an erosion of, or augments, the width of an etched region. The width of the error is assumed to have a zero-mean normal distribution of defined standard deviation. The DOE ideal structure and the error function are each Fourier transformed, summed and modulus squared in order to assess the effects of the plotting error. This model is amenable to numerical evaluation and for comparison with a computer simulation. The results indicate that for a $25\mu\text{m}$ period grating a $1\mu\text{m}$ (or $0.5\mu\text{m}$) plotting error will lead to a variation of the relative energy scattered into each diffraction order with an average rms of 6.2% (or 1.6%). This error can be reduced by plotting the masks with higher precision, e.g. using electron-beam lithography. However, that is significantly more expensive than the laser-plotting here.

3.10. Errors – summary

We have discussed the principal sources of error and have assessed their significance using ray-tracing, theoretical analyses and computer simulations. We find that with achievable accuracies, the etch-depth error, the residual surface roughness, the thickness of the spectral filters and DOE substrate, the misplacing of the grating and the delivery of images in the ± 1 diffraction order do not produce significant image defects. We find that the image sharpness is a good experimental measure to characterize 'best focus'. We find that the axial spacing and location of the in-focus images are altered slightly by the use of thick lenses and the aberrations introduced by other optics. The principal influence on the ability to balance the energy in the multi-focal images arises from the slight change in the NA of the imaging system between diffraction orders of the DOE. For narrow-spectral bands the plotting accuracy dominates other errors, but the analysis here was in 1D and we expect this effect to be less in 2D DOEs. The most serious error in fluorescence imaging arises from the wavelength-dependent diffraction

angle of the ± 1 diffraction orders. In multi-focal imaging this effect may be largely corrected by pre-dispersing the light before it strikes the DOE [2], however, work continues to find a telecentric and high-efficiency implementation of this.

4. TRACKING

Image sharpness has been shown to provide a simple algorithm for the accurate determination of the depth of a particle to be tracked. Experimental measurements on high-brightness sources [5, 6] have demonstrated a tracking accuracy of $\pm 8\text{nm}$ in a single data frame and modeling has indicated that a flux of 200 detected photons should permit particle-tracking with an instantaneous tracking error of less than 30nm . The tracking scheme assesses depth by combining the image sharpness in images focused at three different depths within the specimen. The method uses experimentally-calibrated data, is largely insensitive to the various errors discussed here and can be combined with (x,y) tracking [10].

5. LIST OF SYMBOLS

wavelength	λ ,	nm
etch depth	ϵ ,	μm
refractive index	n ,	
phase angle	φ ,	rad
focal length	f ,	mm
Strehl ratio	S ,	
phase variance	σ_φ^2 ,	rad^2
standard deviation of roughness	σ_ϵ ,	nm

REFERENCES

- [1] Bucklew, J., Gallagher, N.: *Detour phase error in the Lohmann hologram*, Applied Optics, Vol. 18 (1979), p. 575-580
- [2] Blanchard, P. M., Greenaway, A. H.: *Simultaneous multiplane imaging with a distorted diffraction grating*, Applied Optics, Vol. 38 (1999), p. 6692-6699
- [3] Blanchard, P. M., Greenaway, A. H.: *Broadband simultaneous multiplane imaging*, Optics Communications, Vol. 183 (2000), p. 29-36
- [4] Djidel, S., Gansel, J. K., Campbell, H. I., Greenaway, A. H.: *High-speed, 3-dimensional, telecentric imaging*, Optics Express, Vol. 1 (2006), p. 8270-8277

- [5] Dalgarno, P. A. *et al*: *Multiplane imaging and three-dimensional nanoscale particle tracking in biological microscopy*, Optics Express, Vol. 18 (2010), p. 877-884
- [6] Dalgarno, H. I. C. *et al*: *Nanometric depth resolution from multi-focal images in microscopy*, J. R. Soc. Interface, Vol. 8 (2011), p. 942-951
- [7] Born, M., Wolf, E.: *Principles of optics*, Pergamon, London, 1959
- [8] Thompson, M. A. , Lew, M. D., Badieiorstami, M., Moerner, W. E.: *Localizing and tracking single nanoscale emitters in three dimensions with high spatiotemporal resolution using a double-helix point spread function*, Nano Lett., Vol. 10 (2010), p. 210-218
- [9] Muller, R. A., Buffington, A.: *Real-time correction of atmospherically degraded telescope images through image sharpening*, J. Opt. Soc. Am., Vol. 64 (1974), p. 1200-1210
- [10] Yang, L., Lu, W., Yang, J.: *A new tracking method for small infrared targets*, Proc. IEEE Int. Conf. Image Proc. (ICIP), Cario, 2009, pp. 3609-3612

Received:
11. 11. 2011.

Accepted:
30. 11. 2011.

Authors' address

Yan Feng
Louisa Scholz
Heather Dalgarno
David Foo
Lei Yang
Weiping Lu
Alan Greenaway
Physics, SUPA/IIS, School of Engineering and Physical Sciences, Heriot-Watt University, Edinburgh
EH14 4AS
United Kingdom
David Lee, Optical Design Engineer
UK Astronomy Technology Centre
Blackford Hill, Edinburgh
EH9 3HJ
United Kingdom
Heather Dalgarno, Research Associate
Dept of Physics and Astronomy, St Andrews University, North Haugh, Fife
KY16 9SS
United Kingdom
yf47@hw.ac.uk
scholz.louisa@web.de
david.lee@stfc.ac.uk
hicd2@st-andrews.ac.uk
D.M.H.Foo@hw.ac.uk
L.Yang@hw.ac.uk
W.Lu@hw.ac.uk
A.H.Greenaway@hw.ac.uk

